

Electrically controlled waveguide polariton laser

D. G. Suárez-Forero,¹ F. Riminucci,^{2,3} V. Ardizzone,^{1,*} M. de Giorgi,¹ L. Dominici,¹
F. Todisco,¹ G. Lerario,¹ L. N. Pfeiffer,⁴ G. Gigli,² D. Ballarini,¹ and D. Sanvitto^{1,†}

¹*CNR NANOTEC, Institute of Nanotechnology, Via Monteroni, 73100 Lecce, Italy*

²*Dipartimento di Fisica, Università del Salento, Strada Provinciale Lecce-Monteroni, Campus Ecotekne, Lecce 73100, Italy*

³*Molecular Foundry, Lawrence Berkeley National Laboratory,
One Cyclotron Road, Berkeley, California, 94720, USA*

⁴*PRISM, Princeton Institute for the Science and Technology of Materials, Princeton University, Princeton, NJ 08540*

Semiconductor polariton systems offer a versatile solid state platform to study many-body physical effects such as lasing or superfluidity in out-of-equilibrium systems. They are also anticipated as a new platform for integrated optics: behaving as interacting photons, these mixed light-matter quasi-particles could be the cornerstone of a new technology for optoelectronic devices, implementing logic gates, switches and other functionalities. In this work we demonstrate an electrically controlled polariton laser, in a compact, easy-to-fabricate and integrable configuration, based on a semiconductor waveguide. Interestingly, we show that polariton lasing can be achieved in a system without a local minimum in the polariton energy-momentum dispersion. The surface cavity modes for the laser emission are obtained by adding couples of specifically designed diffraction gratings on top of the planar waveguide, forming an in-plane Fabry-Perot cavity. It is precisely thanks to the waveguide geometry, that we can apply a transverse electric field in order to finely tune the laser energy and quality factor of the cavity modes. Remarkably, we exploit the system sensitivity to the applied electric field to achieve an electrically switched source of coherent polaritons. The precise control that can be reached with the manipulation of the grating properties and of the electric field, provide strong advantages to this device in terms of miniaturization and integrability, two main features for the future development of coherent sources from polaritonic technologies.

INTRODUCTION

A semiconductor system in which a photon emitted from an active medium has a larger probability of being reabsorbed than that of escaping out of the optical resonator, is called to be in strong coupling. This condition translates for the formation of the so called exciton polariton: a light-matter quasi-particle resulting from the hybridization between an electromagnetic cavity mode and an exciton dipole in a semiconductor [1]. Since the first observation [2], polaritonic systems have become a suitable platform to study fundamental physical phenomena; effects such as optical parametric oscillations [3], bistability [4], Bose-Einstein condensation [5, 6], superfluidity [7, 8] and quantum vorticity [9] are some of the most intriguing phenomena that have been demonstrated. Peculiar features of polaritons such as long coherence time and high nonlinearities are chased for the realization of integrated optical elements [10]. Experimental devices such as polariton transistors [11] and routers [12] have indeed shown their viability for all-optical logic systems. More recently, the generation and manipulation of polaritons at the single or few particles level, have been reported [13–15], in an effort to assess the potential of these systems as a platform for quantum information processing.

The so called “polariton laser” [16] is one of the most paradigmatic effects observed in strongly coupled systems. This phenomenon is observed when a phase transition to a coherent state of polaritons takes place above a critical density. It has been demonstrated in systems such as semiconductor, organic or hybrid microcavities [17–24] and photonic crystal cavities [25–27]. From this point of view, optical waveguides (WG) represent a very attractive platform for the exploitation of this effect in actual devices, due to an easy technological fabrication, the high quality factors achievable and the particular geometry, suitable for the integration of polaritonic optical circuits and coherent optical sources. A guided electromagnetic mode, localized in the two dimensional plane of the WG by total internal reflection, couples to an exciton which is confined to the quantum well (QW), giving rise to WG polariton modes [28], in counterposition to the more reknown microcavity polariton modes [1]. We indeed show that, despite the lack of an energy minimum in the WG polariton dispersion, an electrically controlled polariton lasing effect can be achieved even with guided polaritons propagating at high speed.

We use two metal gratings placed on top of the GaAs/AlGaAs slab, that behave like a couple of semi-reflective mirrors, confining the WG polariton mode, and furthermore to outcouple the laser emission vertically throughout one of their diffraction orders. Their design favors the formation of an energy gap in the energy momentum dispersion of the planar WG mode. Inside this energy interval, a manifold of Fabry-Perot (FP) modes is formed by the cavity effect between the gratings, funneling the light absorbed and reemitted by carrier recombinations under the pump

spot. The lasing effect is then enabled on a specific polariton mode, i.e., the first mode for which gain equals losses upon increasing pump power. Parameters such as grating periodicity and filling factor as well as the cavity length (i.e. distance between gratings) provide a fine control of the laser properties, without the need for complex postprocessing of the WG. Most importantly, using an electric field applied in the direction perpendicular to the WG plane, we demonstrate real-time tunability of the emission wavelength. We stress that this electrical control is possible only because of the WG geometry, that allows to place the electrodes in close vicinity to the quantum wells. The strong coupling regime and the sensitivity of the exciton to the externally applied electric field allow us to obtain an electrically controlled source of coherent polaritons, realizing electro-switching with ultra-high figures of merit. Based on these findings, the coherent, electrically controlled polaritons source demonstrated here could be an important tool for future polariton circuits, enabling functionalities such as electrical injection, Q-switch lasers, electro-optic modulators and configurable logic gates.

RESULTS

The WG structure is grown on an n^+ -doped GaAs substrate, on top of which a 500 nm cladding of $Al_{0.8}Ga_{0.2}As$ was previously deposited. The structure consists of 12 pairs of 20 nm thick GaAs quantum wells (QW) separated by 20 nm of $Al_{0.4}Ga_{0.6}As$ barriers. Light is extracted through gold gratings spaced by a distance ranging from 50 μm to 150 μm . To realize FP resonators inside the WG, two identical gratings are fabricated facing each other on top of the slab at a given distance along their line of sight (a sketch of the full system is shown in Fig. 1a). We use gratings with pitch ~ 240 nm and filling factor comprised between ~ 0.65 and ~ 0.72 . Finally, a 50 nm layer of ITO is sputtered on top of the sample. This layer, together with the doped substrate in the opposite side, allows for the application of an electric field in a direction perpendicular to the slab plane. The purpose of the electric field is to tune the exciton energy, exploiting the Stark effect, and hence its influence on the polaritonic guided modes. A more detailed description of the structure is given in the Materials and Methods section.

To firstly verify the presence and features of the WG modes inside the slab, we use a non-resonant pump laser which excites the sample outside of the gratings region, while the photoluminescence (PL) spectrum of the system is collected through an individual grating (so no cavity is formed) placed 100 μm away from the off-resonant excitation spot. Figure 1b shows the PL emission coming from the zero-th order Transverse Magnetic (TM) mode of the structure, while Fig. 1c shows the corresponding emission coming from the zero-th order Transverse Electric mode (TE). The dispersions are plotted as a function of the wavevector β of the propagating mode inside the slab. The uncoupled bare exciton line (heavy hole exciton) and guided optical modes are indicated by horizontal and oblique red dashed lines, respectively. The experimental polariton dispersion can be fitted by means of a theoretical model of coupled oscillators, as shown by the solid lines in Fig.1b-c. The results show an asymmetry in the Rabi splitting (Ω) between the TE and TM modes. We obtain values of 13.4 meV and 5.2 meV, respectively. As a matter of fact this is predicted by the selection rules for the coupling of the confined modes with the exciton dipole, which imply an Ω value around three times higher for the TE mode than for the TM mode, as it has already been observed in similar samples [29, 30]. The figure also evidences an important difference in the wavevector β spreading between the TM and the TE modes. This linewidth effect is originated by the different grating efficiency with respect to each polarization and it is correlated with the formation of the FP cavity inside the structure, as will be described in detail in the Discussion Section.

After the WG modes, we also characterize the features of the top gratings and their role in forming the the FP cavity. Figure 2a shows the angle-integrated PL emission intensity from the terminal end of a single and very extended, 400 μm -long grating as a function of the emission energy. Both the TE and TM polarization possess a local minimum in the emitted intensities, highlighted by vertical arrows in the figure. These minima represent energy gaps corresponding to wavevectors of the guided modes that are back-reflected by the grating. In other words, each grating acts as a mirror in the energy interval corresponding to the gaps of Fig. 2a and, when two gratings face each other, a planar FP cavity is formed, with a cavity length which depends on the distance L between gratings. The cavity modes are characterized now thanks to the PL emission outcoupled from one of the gratings when non-resonantly exciting in the middle between the two. Figure 2b shows the PL emission of the cavity modes formed by placing the gratings at distances of $L = 50$ μm (black upper line), $L = 100$ μm (middle blue line) and $L = 150$ μm (lower red line). As expected, the closer the gratings to each other, the larger the free spectral range. In the case of the gratings separated by 50 μm the modes spacing is ~ 2.3 meV that corresponds to the FP mode of manifold 17. For the case of a pair of gratings separated 100 μm , the spacing is ~ 1.4 meV (manifold 30) and for the gratings separated 150 μm the spacing is ~ 0.9 meV (manifold 45). These FP modes, which arise from the confinement of the TM guided mode, are directly related to the interaction of the field with the diffraction grating. In fact, the TM dispersion changes considerably

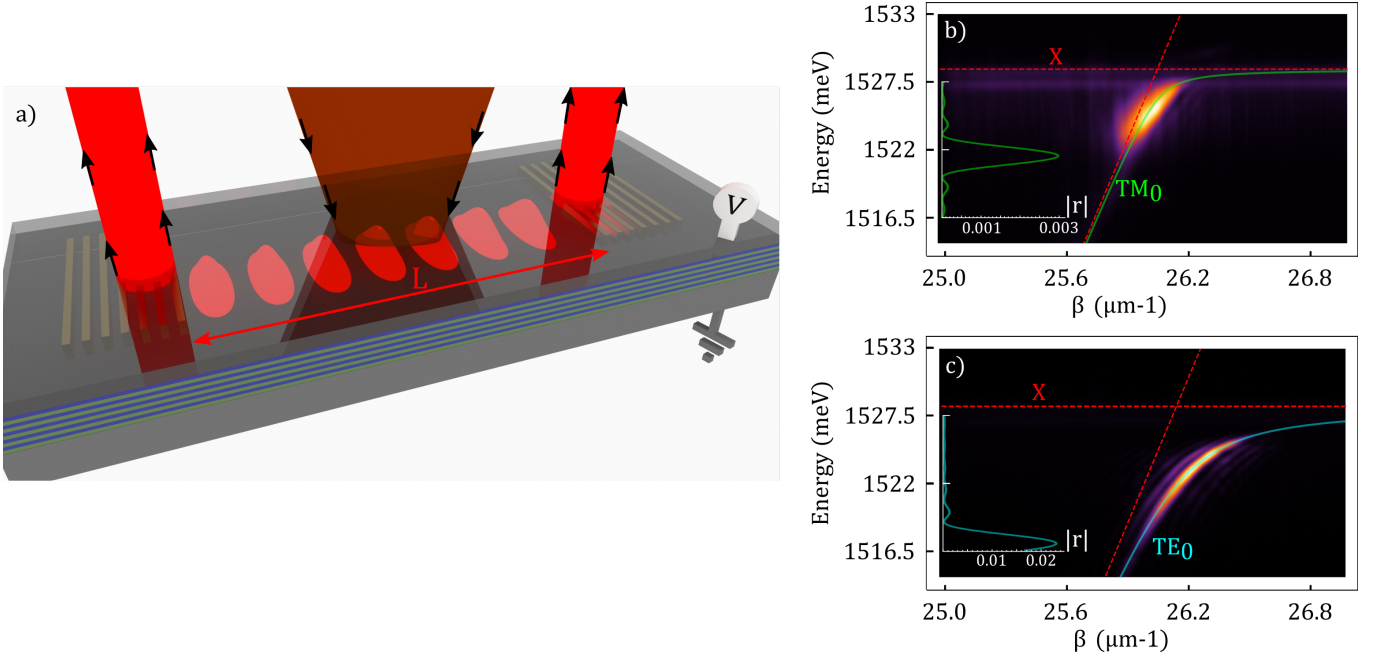


FIG. 1. **a** Schematic representation of the system. Two gold gratings, placed on top of the WG, couple to the vanishing tail of the guided modes. As a result, a FP cavity is formed inside the slab for the TM mode, opening the possibility to observe a lasing effect in the system. L is the cavity length given by the distance between the gratings. The doped substrate, together with a top layer of ITO, enables the application of an electric field in the direction perpendicular to the cavity plane. **b-c** Polarization resolved PL dispersion of the system extracted through a single gold grating placed on top of the slab WG. The dispersion are plotted as a function of β the wavevector of the guided modes. Panel a corresponds to TM polarization, while panel b shows the dispersion for the TE mode. Continuous lines correspond to a fitting of each mode by using a theoretical model of coupled oscillators. The obtained Rabi splitting (Ω) values are 5.2 meV for the TM mode and 13.4 meV for the TE. The bare exciton and photonic modes are indicated by the red dashed lines. The calculated reflectivity of the grating is displayed for each polarization. The insets represent the calculated reflectivity of each grating in both TE and TM polarization, showing the opening of an energy gap.

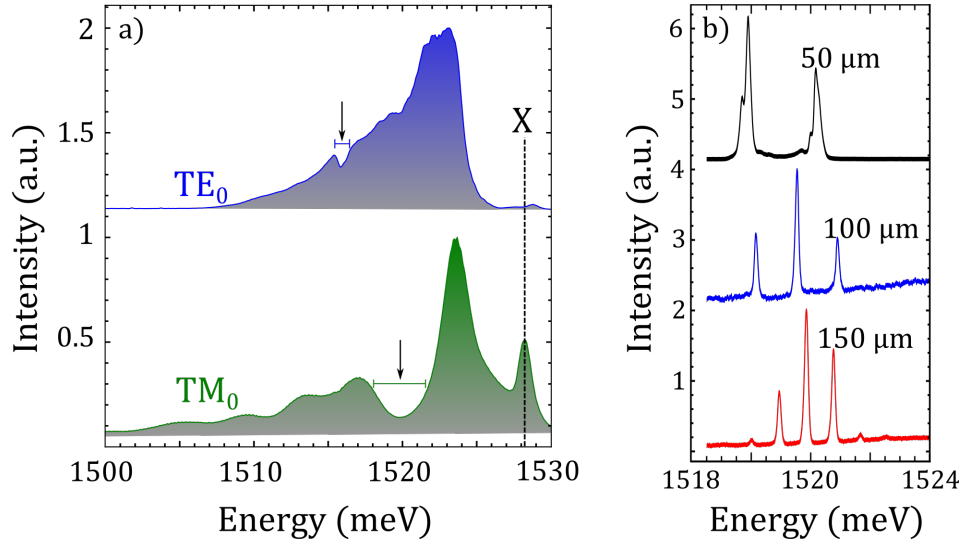


FIG. 2. **a** Experimental measurement of the gratings gap in TE and TM polarization. The spectra are obtained by integrating the PL emission from the terminal end of a 400 μm -long gold grating over the emission angle. The vertical dashed line indicates the exciton energy. The opening of two bandgaps is highlighted by the vertical arrows. **b** Fabry-Perot modes registered in cavities of different length, determined by the distance between the gratings. As expected for an optical cavity, the smaller the cavity, the greater the free spectral range at a given energy. The spectral distances of 2.3 meV for the cavity of length 50 μm , 1.4 meV for the cavity of 100 μm and 0.9 meV for the cavity of 150 μm , are associated to FP modes of manifold 17, 30 and 45, respectively.

when extracted through a much less perturbative grating fabricated on a 50 nm layer of ITO on top of the slab, instead of being in direct contact with the WG (Fig. S2). We attribute both the strong effect of the grating on the TM mode, and the wider energy gap respect to the TE mode (Fig. 2a), to a plasmonic contribution due to geometry reasons. The grating is composed of gold nanowires about 174 nm wide; for this structure, a well known plasmonic modulation of the refractive index for the TM polarized electromagnetic field takes place in the near infrared [31–33].

We have till now characterized all the three building blocks (namely the WG modes, the gratings and the planar cavity), which are mandatory for the observation of the waveguiding lasing effect. We can hence shine a high peak-power non-resonant laser in a region between the two gratings, in the specific we use a 100 fs pulsed laser tuned at 1.59 eV (≈ 780 nm) and 80 Mhz repetition rate, with a spot size of 40 μm . Figure 3a shows the PL emission in real space at threshold excitation power. The big spot between the gratings corresponds to the exciton emission under the pump spot which is not coupled to the guided modes. The excited guided polariton modes propagate along the slab with in-plane vector β and are partly extracted and partly reflected back in the plane when they hit the gratings, highlighted by white rectangles. The PL emission extracted from grating 1 can be resolved in both energy and momentum (Fig. 3b). Remarkably, such emission shows a series of discrete peaks along the TM polariton dispersion corresponding to the FP modes of Fig. 2b. In other words, in the region of space comprised between the two identical gratings, a FP cavity is formed, sustaining the discrete modes observed in Fig. 3b. With increasing pump power, as shown in Fig. 3c-d, the system shows a clear threshold behaviour (see inset of panel d) with prominent coherent emission from only one of the FP modes. When the light from the two gratings is overlapped in k space, an interference pattern is generated (Fig. S3a). Moreover, a strong reduction of the linewidth of the FP mode is observed across the lasing threshold (Fig. S3b). The threshold and linewidth effects are clear signatures which mark the onset of the lasing regime in the system. We gain an even better insight into the laser emission build-up, upon accessing the temporal dynamics of the process by means of a streak camera coupled to a monochromator and a scan in the reciprocal space. The energy momentum dispersion resolved at different time frames of the dynamics is shown in the Supplementary Video 1 and discussed in the Supplementary Material, along with a detailed screenshot in Fig. S4. In this case the pump spot is placed between the two gratings and the emission from one of the gratings is recorded. The maximum population in the laser mode is reached 200 ps after the pulse arrival. Taking into account that its group velocity, deduced as the first order derivative of the energy dispersion from the theoretical fit of the measured dispersions, is around 55 $\mu\text{m}/\text{ps}$, it is possible to conclude that the stimulated emission process requires a few hundreds of round trips of the initial pulse inside the cavity before reaching the stimulated emission regime. In the supplementary Video 2 we show the dynamics of the system measured under the pumping laser, by placing its spot on one of the two gratings and imaging the emission from both (see Fig. S5 for the experimental details). Supplementary Video 2 shows that under the pumping spot the strong exciton-photon coupling is lost when the excitation pulse arrives, essentially due to the high density of photo-generated carriers, and then is slowly recovered after the lasing action is over. The system is excited at threshold, which explains why several FP modes are still visible. On the lower part of the image, the TE polariton mode is also visible however this mode comes from the grating at the opposite side of the excitation spot, thus always in the strong coupling regime. Two screenshots taken from the video are reproduced and detailed in the Supplementary Material, Figs. S4 and S5.

Finally, we can now apply an external electric field perpendicular to the plane of the slab, demonstrating an extra degree of freedom acting as an additional control parameter on the WG polariton lasing. Figure 4a shows the spectra obtained from the TM polariton dispersion at $\beta \approx 25.8 \mu\text{m}^{-1}$ and for different applied voltages. The TM dispersion is modified due to the Stark effect that red-shifts the exciton energy, providing a tool for a fine tuning of the laser energy in real time. In Fig. 4b-c we measure the central emission energy and the linewidth of the lasing mode for three different applied voltages and as a function of the pump power. For small applied fields (≤ 0.9 V), a red-shift of the lasing mode is observed. When the applied electric field is further increased (> 0.9 V), the exciton energy approaches the cavity modes, more largely altering their absorption properties, and hence, their relative losses. As a matter of fact, Fig. 4d shows that for an applied voltage of 1.5 V, the mode in which the stimulated emission takes place jumps to the next manifold. Both spectra of figure Fig. 4d are taken at threshold power. The applied electric field acts in this case as a neat switch that allows to select the mode in which the lasing takes place. While at low voltages the electric field provides a fine control over the laser central energy, at higher fields a further increase in the intensity allows for abrupt changes of the lasing line, by modifying the FP modes relative losses. The inset of Fig. 4d shows the evolution of the linewidths of the two lasing peaks upon application of the electric field. Indeed the switch between the lasing modes also coincides with the crossing of their linewidths.

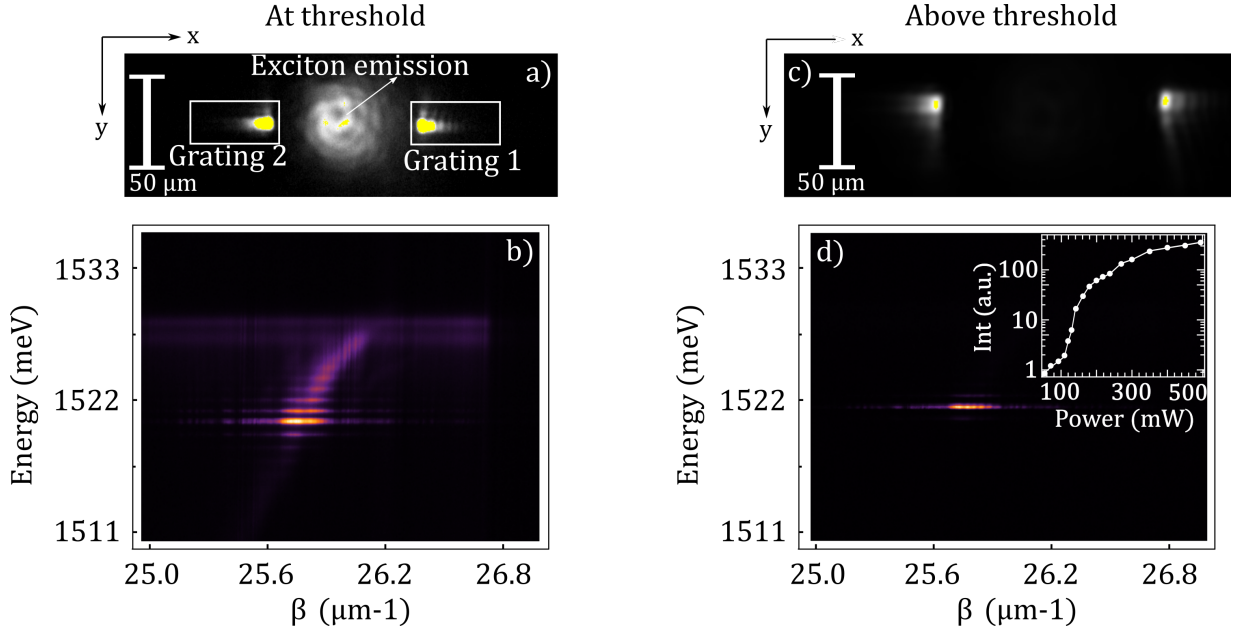


FIG. 3. **a** Real space image of the system when excited out of resonance at the threshold power. The laser spot is placed in the middle of the FP cavity, exciting both, the QW exciton with low in-plane momentum (central spot) and the polaritonic guided modes, extracted from the gratings (indicated with white rectangles). The residual pump laser signal is suppressed with a long-pass spectral filter. **b** The TM mode is reconstructed in the Fourier space by spatially isolating the PL from grating 1. The insertion of the gratings entails an additional confinement, and hence, the formation of discrete modes along the TM dispersion, as it can be observed in the image. **c** When the pump power overcomes the threshold, one mode of the cavity gets massively populated, reaching an emission intensity much higher than any other emission in the system. **d** the PL dispersion measurement (measured as in **b**) confirms which state of the FP cavity gets populated. The inset in **d** shows the intensity of the lasing mode as a function of the pumping power; a clear threshold behaviour is visible.

DISCUSSION

We demonstrated the design and realisation of a micrometer size laser in a GaAs/AlGaAs polariton-WG by using two metallic gratings at controlled distance on top of the slab WG, in order to form a FP cavity that confines the photonic field in one dimension. To better understand this effect, we calculate the influence of the grating on the guided modes by using a perturbation formalism to study the coupling between counter-propagating modes [34, 35]. For a WG grown in the x direction, and with modes propagating in the z direction, the magnetic field $H(x, z, t)$ of the m^{th} TM mode, can be expressed in case of an infinite slab in the y direction (i. e. $d/dy = 0$) as:

$$H_m(x, z, t) = \mathcal{H}_y^m(x) e^{i(\omega t - \beta_m z)} \quad (1)$$

Where $\mathcal{H}(x)$ is derived from the corresponding wave equation and boundary conditions. A more detailed explanation, based on ref. [36] is included in the SM. The fabrication of a grating with periodicity Λ on top of the WG acts as a perturbation that changes the effective in-plane momentum of the m^{th} mode as:

$$\beta'_m = \frac{l\pi}{\Lambda} - \sqrt{\left(\beta_m - \frac{l\pi}{\Lambda}\right)^2 - |\kappa|^2} \quad (2)$$

With β_m the in-plane momentum of the unperturbed m^{th} mode, l an integer number such as $|\beta_m - \frac{l\pi}{\Lambda}| \sim 0$ and κ a constant that depends on the grating periodicity and material, and the spatial profile of the transverse field. In the case of a square grating fabricated on top of the slab, with filling factor a , height h and refractive index n_g , the constant κ takes the form

$$\kappa = \frac{i\omega\mu_o}{4\pi l} \sin(\pi l a) \int_0^h \left((n_g/n_{ITO})^2 - 1 \right) [\mathcal{H}_y^m(x)]^2 dx \quad (3)$$

This expression indicates the existence of an energy gap in the guided mode dispersion in the region covered by the grating when $|\kappa|^2 > \left(\beta_m - \frac{l\pi}{\Lambda}\right)^2$. At the energy interval around the exciton (~ 1.529 meV), where the electromagnetic

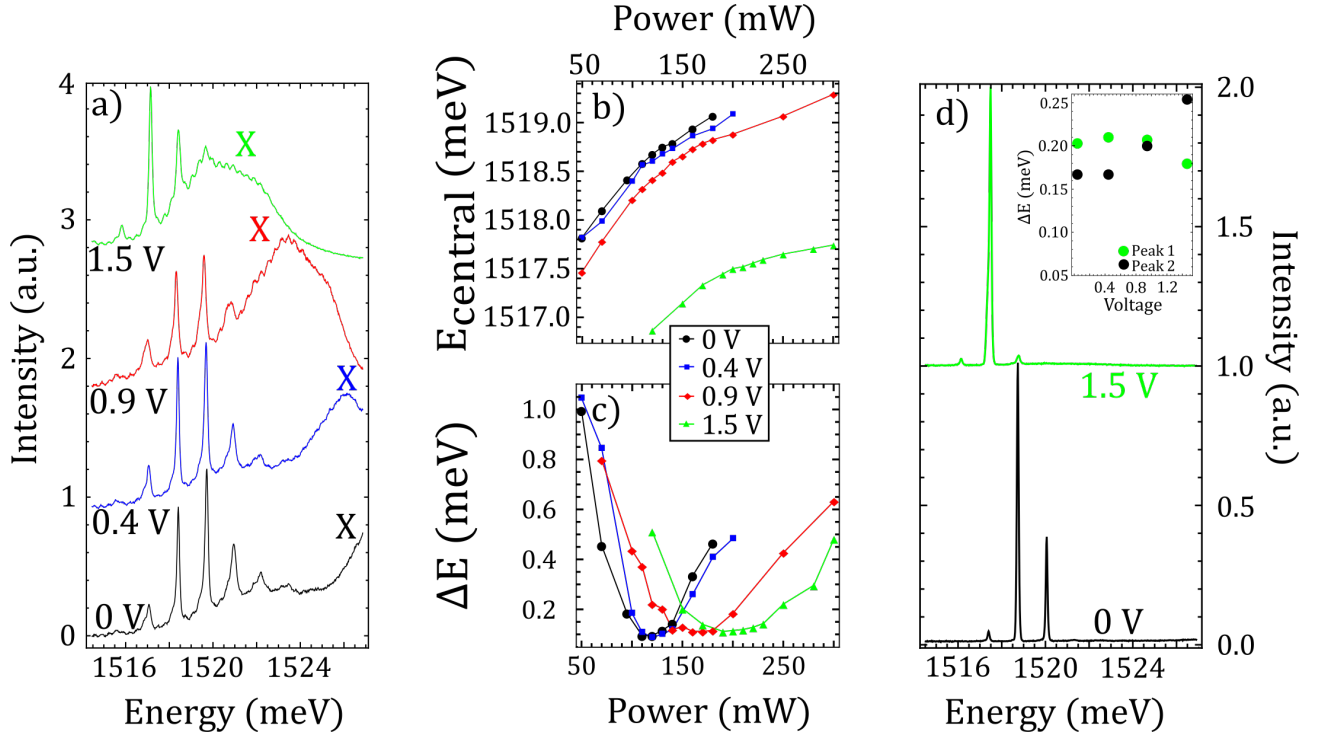


FIG. 4. **a** Spectra obtained by cutting the TM polariton dispersion at $\beta \approx 25.8 \mu\text{m}^{-1}$ and for different applied voltages. The letter X indicates the peak corresponding to the PL emission of the uncoupled exciton which redshifts due to the Stark effect. **b** and **c** To verify that the presence of a transverse electric field does not affect the properties of the lasing effect, we verify the central energy shift (**b**) and spectral narrowing (**c**) for three applied voltages. The results not only confirm the lasing effect in every case, but show that the electric field acts as a fine tuning of the laser energy for small voltages through the Stark shift of the exciton, and as a switch that allows to select the cavity mode in which the lasing will take place. The latter effect is achieved as a consequence of a modification of the relative Q factor of the cavity modes, since the exciton resonance affects the absorption at the energy of the lasing FP mode. **d** Spectra of the cavity taken at threshold power without any transverse electric field (black) and with an applied voltage of 1.5 V (blue). The modes energy is almost unaltered, but the change of their absorption properties switches the mode in which the stimulated emission takes place. The inset shows the FWHM of each peak as the applied electric field increases. When the quality factor of peak 1 decreases below the one of peak 2, the lasing effect takes place on peak 2.

field hybridizes, the in-plane linear momentum of the TM guided mode lies in the range ($25.6 \mu\text{m}^{-1} < \beta_m < 26.3 \mu\text{m}^{-1}$), as observed in Fig. 1b. For a grating with a period of $\Lambda = 243 \text{ nm}$, the condition $\beta_m - \frac{l\pi}{\Lambda} \sim 0$ is satisfied for $l = 2$. The expressions 3 shows that, for l even, κ differs from zero only for filling factors different than 0.5. Moreover it is also evident from the expressions that for $l = 2$ the maximum gap's amplitude is obtained for a filling factor either 0.25 or 0.75. In our case, we fabricated gold gratings with filling factor close to 0.75 to maximize the coupling between propagating and counter-propagating modes and hence their reflectivity, whose calculation is shown on the left side of Figs. 1b and 1c. In summary, by engineering the parameters of the metallic gratings pairs such as relative distance, periodicity and filling factor, we obtain a fine control of the system's properties without the need for any modification in the slab WG.

It is worth noting that the blueshift of Fig. 4b cannot be simply associated to polariton-polariton interactions, since the exciton energy remains almost unaltered when the pump power is increased. It rather might depend on a local carrier-induced reduction of the WG's refractive index [37], due, for example, to the plasma generated by the optical pump pulse, i. e., a plasma induced transparency [38, 39] or to the band filling effect. Such effects can be especially relevant in the spatial region below the pump spot. An estimation of the minimum index change necessary to account for the observed blueshift with increasing pump power can be done by considering that the i^{th} mode of the resonator has energy $E_i = i \frac{h \cdot c}{2Ln}$, where L is the cavity length, given by the distance between the gratings, n its effective refractive index, h the Planck's constant and c the vacuum light speed. The data shows a saturation behavior compatible with such explanation, with a reduction of only 10^{-4} in the refractive index. Figure 4c shows the linewidth for different pump powers and voltages. The observed spectral narrowing at threshold is expected and it is

associated to the fact that the coherence time of the system exceeds the radiative lifetime of the confined mode under these excitation conditions [17]. Based on the complex temporal dynamics that we observe in the Supplementary Videos 1 and 2, we can explain the laser build-up in the following way. When a pump pulse arrives in the region between the gratings, a spatially localized population inversion is created. Part of the energy coming from the carriers recombination is injected into the guided polaritonic modes and funneled into the FP modes formed by the two gratings (see Fig. 3a). Among the several FP modes in which light is injected, the first to realize the balance between gain and losses reaches the lasing threshold and becomes massively populated (Fig. 3b). In the polariton laser we report here, a spatially localized population inversion is formed and coherently populates a guided polariton mode outside of the pumping region. In fact, as the two videos and related figures S4 and S5 show, in our WG a spatially localized weak-coupling region coexists with a strongly coupled mode away from the pumping region. This scheme gives rise to a source of high-speed coherent polaritons. We note also that recently a polariton laser effect has been claimed at both cryogenic and room temperature in ZnO based WGs [40]. In that case, the polariton emission has been interpreted as a standard polariton laser without need for a population inversion. While this interpretation can be supported by the large Rabi splitting observed in ZnO systems, our present work shows that in guided polariton systems an alternative interpretation can explain the same features. Moreover the absence of a blueshift in case of Ref. [40] could be also compatible with a refractive index change in the region between the two cracks. A careful check of the dynamics both below and outside the pumping region is essential in this kind of systems to better clarify the lasing mechanism involved.

We also exploit the application of a transverse electric field as a fine real-time tuning of the emission energy or as a switch to select the confined mode on which the stimulated emission takes place. As it is shown in Fig. 4b, when the applied electric potential is smaller than 1V, a small red-shift of the lasing mode is observed. This effect is mainly due to the Stark shift of the exciton, which slightly increases the refractive index at the energy of the FP modes. Moreover, when the exciton energy approaches the lasing mode, the losses due to excitonic absorption increase. This mechanism is responsible for the switching of the lasing mode shown in Fig. 4d. In this case, excitonic losses at 1.5 V modify the quality factor of the modes and the first mode to lase is different from the 0 V case. This interpretation is confirmed by studying the FWHM of the two peaks, shown in the inset of the figure. As the applied electric potential increases, the linewidth of the peak lasing at 0V (Peak 2) increases until it becomes larger than the linewidth of the peak lasing at 1.5V (Peak 1). The application of the electric field is then equivalent to an external control of the quality factor of the FP modes and it allows the selection of the lasing mode.

In summary, we report a lasing effect providing a coherent source of high-speed, guided polaritons. The additional optical confinement necessary to achieve the laser emission is provided by placing two specifically designed gold gratings on top of the WG. It is worth to note that this design is versatile, easy-to-fabricate and does not require complex post-processing of the WG, such as vertical selective etching. Most important, thanks to the WG geometry, we demonstrate an effective electrical control of the vertical laser emission. Remarkably, by electrically tuning the quality factor of the modes, we obtain an electrically switched polariton laser. This effect could be exploited for the realization of electrically Q-switched sources of polaritons. More generally, the lasing effect we report in this work would allow the construction of tunable, micrometer-size coherent sources of polaritons with different properties in a single wafer of slab WG. These kind of optical sources could be valuable in polaritonics especially in the development of polaritonic circuits and integrated polaritonic logic elements.

MATERIALS AND METHODS

Waveguide sample The full structure is grown on top of an n^+ -doped GaAs substrate 500 μm thick. The cladding layer is made of 500 nm of $\text{Al}_{0.8}\text{Ga}_{0.2}\text{As}$, while the WG is composed by 12 bilayers of $\text{Al}_{0.4}\text{Ga}_{0.2}\text{As}$ (20 nm thick) and GaAs (20 nm thick), and a final bilayer made of 20 nm of $\text{Al}_{0.4}\text{Ga}_{0.2}\text{As}$ and 10 nm of GaAs.

Fabrication of gold gratings and deposition of ITO In order to fabricate gold gratings onto the sample we relied on a lift-off process. The designed gratings are 100 μm long, 50 μm wide and they are characterised by a pitch of 243 nm. The gratings are grown with a length of 100 μm . Their production requires a positive e-beam resist PMMA A4 to be spun at 4000 rpm onto the sample and baked for three minutes at 180 $^\circ\text{C}$. The latter is then exposed using Raith150 and developed in MIBK:IPA 1:3. Subsequently, 3 nm of chromium and 30 nm of gold are thermally evaporated. The sample is placed in Remover PG at approximately 80 $^\circ\text{C}$ to remove the resist. In closing, the electric contact is obtained by uniformly sputtering 50 nm of Indium Tin Oxide (ITO) on top of the sample; the gold grating

results completely covered in the end.

Optical measurements For all the optical characterization the sample is kept at cryogenic temperature of 4 K. All the PL measurements are realized in a confocal configuration, using a 100 fs pulsed laser with a repetition rate of 80 MHz, tuned at 1.59 eV (≈ 780 nm) to excite the sample out of resonance. The detection system allows to reconstruct either real or Fourier spaces in a Charge Coupled Device (CCD) coupled to a monochromator 70 cm long with a diffractive grating with either 600 or 1800 lines per mm. This way it is possible to perform measurements resolved in space, angle and energy. An image of the real space is reconstructed before the CCD in order to apply a spatial filter by using a slit, enabling the selection of one or both gratings. The residual laser signal is suppressed with a long-pass spectral filter at 1.55 eV (≈ 800 nm). The time resolved images are performed in the same configuration, but directing the signal into a streak camera after passing the monochromator. The temporal reconstruction of the far field resolved in energy is made by moving vertically the focusing lens with a motorized station before it reaches the streak camera.

Acknowledgments We thank Paolo Cazzato for the technical support.

Work at the Molecular Foundry was supported by the Office of Science, Office of Basic Energy Sciences, of the U.S. Department of Energy under Contract No. DE-AC02-05CH11231.

We acknowledge the project FISIR - C.N.R. Tecnopolo di nanotecnologia e fotonica per la medicina di precisione - CUP B83B17000010001 and "Progetto Tecnopolo per la Medicina di precisione, Deliberazione della Giunta Regionale n. 2117 del 21/11/2018.

* v.ardizzone85@gmail.com

† daniele.sanvitto@nanotec.cnr.it

- [1] Alexey Kavokin, Jeremy J. Baumberg, Guillaume Malpuech, and Fabrice P. Laussy. *Microcavities*. Oxford Science, second edition, 2008.
- [2] C. Weisbuch, M. Nishioka, A. Ishikawa, and Y. Arakawa. Observation of the coupled exciton-photon mode splitting in a semiconductor quantum microcavity. *Phys. Rev. Lett.*, 69:3314–3317, Dec 1992.
- [3] J. J. Baumberg, P. G. Savvidis, R. M. Stevenson, A. I. Tartakovskii, M. S. Skolnick, D. M. Whittaker, and J. S. Roberts. Parametric oscillation in a vertical microcavity: A polariton condensate or micro-optical parametric oscillation. *Physical Review B - Condensed Matter and Materials Physics*, 62(24):R16247–R16250, dec 2000.
- [4] A. Baas, J. Ph Karr, M. Romanelli, A. Bramati, and E. Giacobino. Optical bistability in semiconductor microcavities in the nondegenerate parametric oscillation regime: Analogy with the optical parametric oscillator [13]. *Physical Review B - Condensed Matter and Materials Physics*, 70(16):1–4, oct 2004.
- [5] J. Kasprzak, M. Richard, S. Kundermann, A. Baas, P. Jeambrun, J. M. J. Keeling, F. M. Marchetti, M. H. Szymańska, R. André, J. L. Staehli, V. Savona, P. B. Littlewood, B. Deveaud, and Le Si Dang. BoseEinstein condensation of exciton polaritons. *Nature*, 443(7110):409–414, sep 2006.
- [6] R. Balili, V. Hartwell, D. Snoke, L. Pfeiffer, and K. West. Bose-Einstein condensation of microcavity polaritons in a trap. *Science*, 2007.
- [7] Alberto Amo, Jérôme Lefrère, Simon Pigeon, Claire Adrados, Cristiano Ciuti, Iacopo Carusotto, Romuald Houdré, Elisabeth Giacobino, and Alberto Bramati. Superfluidity of polaritons in semiconductor microcavities. *Nature Physics*, 2009.
- [8] Giovanni Lerario, Antonio Fieramosca, Fábio Barachati, Dario Ballarini, Konstantinos S. Daskalakis, Lorenzo Dominici, Milena De Giorgi, Stefan A. Maier, Giuseppe Gigli, Stéphane Kéna-Cohen, and Daniele Sanvitto. Room-temperature superfluidity in a polariton condensate. *Nature Physics*, 2017.
- [9] K. G. Lagoudakis, M. Wouters, M. Richard, A. Baas, I. Carusotto, R. André, Le Si Dang, and B. Deveaud-Plédran. Quantized vortices in an excitonpolariton condensate. *Nature Physics*, 4(9):706–710, sep 2008.
- [10] Daniele Sanvitto and Stéphane Kéna-Cohen. The road towards polaritonic devices, 2016.
- [11] D. Ballarini, M. De Giorgi, E. Cancellieri, R. Houdré, E. Giacobino, R. Cingolani, A. Bramati, G. Gigli, and D. Sanvitto. All-optical polariton transistor. *Nature Communications*, 4(1):1778, jun 2013.
- [12] Félix Marsault, Hai Son Nguyen, Dimitri Tanese, Aristide Lemaître, Isabelle Sagnes, Alberto Amo, and Jacqueline Bloch. Realization of an all optical exciton-polariton router. *Applied Physics Letters*, 107(20):201115, nov 2015.
- [13] J.C. López Carreño, C. Sánchez Muñoz, D. Sanvitto, E. del Valle, and F.P. Laussy. Exciting Polaritons with Quantum Light. *Physical Review Letters*, 115(19):196402, nov 2015.
- [14] Á. Cuevas, J.C.L. Carreño, B. Silva, M. De Giorgi, D.G. Suárez-Forero, C.S. Muñoz, A. Fieramosca, F. Cardano, L. Marrucci, V. Tasco, G. Biasiol, E. Del Valle, L. Dominici, D. Ballarini, G. Gigli, P. Mataloni, F.P. Laussy, F. Sciarrino, and D. Sanvitto. First observation of the quantized exciton-polariton field and effect of interactions on a single polariton. *Science Advances*, 4(4), 2018.

- [15] D. G. Suárez-Forero, V. Ardizzone, S. F. Covre da Silva, M. Reindl, A. Fieramosca, L. Polimeno, M. de Giorgi, L. Dominici, L. N. Pfeiffer, G. Gigli, D. Ballarini, F. Laussy, A. Rastelli, and D. Sanvitto. Imaging the hydrodynamics of a single polariton. aug 2019.
- [16] A. Imamoglu, R. J. Ram, S. Pau, and Y. Yamamoto. Nonequilibrium condensates and lasers without inversion: Exciton-polariton lasers. *Physical Review A - Atomic, Molecular, and Optical Physics*, 1996.
- [17] Daniele Bajoni, Pascale Senellart, Esther Wertz, Isabelle Sagnes, Audrey Miard, Aristide Lemaître, and Jacqueline Bloch. Polariton laser using single micropillar GaAs-GaAlAs semiconductor cavities. *Physical Review Letters*, 2008.
- [18] Tsu-Chi Chang, Kuo-Bin Hong, Shuo-Yi Kuo, and Tien-Chang Lu. Demonstration of polarization control GaN-based micro-cavity lasers using a rigid high-contrast grating reflector. *Scientific Reports*, 9(1):13055, dec 2019.
- [19] S. Christopoulos, G. Baldassarri Höger Von Högersthal, A. J D Grundy, P. G. Lagoudakis, A. V. Kavokin, J. J. Baumberg, G. Christmann, R. Butté, E. Feltin, J. F. Carlin, and N. Grandjean. Room-temperature polariton lasing in semiconductor microcavities. *Physical Review Letters*, 2007.
- [20] Gabriel Christmann, Raphaël Butté, Eric Feltin, Jean-François Carlin, and Nicolas Grandjean. Room temperature polariton lasing in a GaNAlGaIn multiple quantum well microcavity. *Applied Physics Letters*, 93(5):051102, aug 2008.
- [21] S. Kéna-Cohen and S. R. Forrest. Room-temperature polariton lasing in an organic single-crystal microcavity. *Nature Photonics*, 2010.
- [22] K. S. Daskalakis, S. A. Maier, R. Murray, and S. Kéna-Cohen. Nonlinear interactions in an organic polariton condensate. *Nature Materials*, 2014.
- [23] T. Guillet, M. Mexis, J. Levrat, G. Rossbach, C. Brimont, T. Bretagnon, B. Gil, R. Butté, N. Grandjean, L. Orosz, F. Réveret, J. Leymarie, J. Ziga-Pérez, M. Leroux, F. Semond, and S. Bouchoule. Polariton lasing in a hybrid bulk ZnO microcavity. *Applied Physics Letters*, 2011.
- [24] Tien-Chang Lu, Ying-Yu Lai, Yu-Pin Lan, Si-Wei Huang, Jun-Rong Chen, Yung-Chi Wu, Wen-Feng Hsieh, and Hui Deng. Room temperature polariton lasing vs photon lasing in a ZnO-based hybrid microcavity. *Optics Express*, 20(5):5530, feb 2012.
- [25] Min Kyo Seo, Kwang Yong Jeong, Jin Kyu Yang, Yong Hee Lee, Hong Gyu Park, and Sung Bock Kim. Low threshold current single-cell hexapole mode photonic crystal laser. *Applied Physics Letters*, 2007.
- [26] Stefano Azzini, Dario Gerace, Matteo Galli, Isabelle Sagnes, Rémy Braive, Aristide Lemaître, Jacqueline Bloch, and D. Bajoni. Ultra-low threshold polariton lasing in photonic crystal cavities. *Applied Physics Letters*, 2011.
- [27] Masahiro Nomura, Naoto Kumagai, Satoshi Iwamoto, Yasutomo Ota, and Yasuhiko Arakawa. Photonic crystal nanocavity laser with single quantum dot gain. In *Optics InfoBase Conference Papers*, 2009.
- [28] P. M. Walker, L. Tinkler, M. Durska, D. M. Whittaker, I. J. Luxmoore, B. Royall, D. N. Krizhanovskii, M. S. Skolnick, I. Farrer, and D. A. Ritchie. Exciton polaritons in semiconductor waveguides. *Applied Physics Letters*, 102(1):012109, jan 2013.
- [29] Itamar Rosenberg, Yotam Mazuz-Harpaz, Ronen Rapaport, Kenneth West, and Loren Pfeiffer. Electrically controlled mutual interactions of flying waveguide dipolaritons. *Physical Review B*, 93(19):195151, may 2016.
- [30] Pavel Yu. Shapochkin, Maksim S. Lozhkin, Ivan A. Solov'ev, Olga A. Lozhkina, Yury P. Efimov, Sergey A. Eliseev, Vyacheslav A. Lovc'jus, Gleb G. Kozlov, Anastasia A. Pervishko, Dmitry N. Krizhanovskii, Paul M. Walker, Ivan A. Shelykh, Maurice S. Skolnick, and Yury V. Kapitonov. Polarization-resolved strong light-matter coupling in planar GaAs/AlGaAs waveguides. *Optics Letters*, 43(18):4526, sep 2018.
- [31] M. W. Klein, T. Tritschler, M. Wegener, and S. Linden. Lineshape of harmonic generation by metallic nanoparticles and metallic photonic crystal slabs. *Physical Review B - Condensed Matter and Materials Physics*, 72(11), sep 2005.
- [32] Xinping Zhang, Shengfei Feng, Jian Zhang, Tianrui Zhai, Hongmei Liu, and Zhaoguang Pang. Sensors based on plasmonic-photonic coupling in metallic photonic crystals. *Sensors (Switzerland)*, 12(9):12082–12097, sep 2012.
- [33] Dominik A. Gollmer, Christopher Lorch, Frank Schreiber, Dieter P. Kern, and Monika Fleischer. Enhancing light absorption in organic semiconductor thin films by one-dimensional gold nanowire gratings. *Physical Review Materials*, 1(5), oct 2017.
- [34] Harold Stoll and Amnon Yariv. Coupled-mode analysis of periodic dielectric waveguides. *Optics Communications*, 8(1):5–8, may 1973.
- [35] A. Yariv. Coupled-mode theory for guided-wave optics. *IEEE Journal of Quantum Electronics*, 9(9):919–933, sep 1973.
- [36] Amnon Yariv and Pochi Yeh. *Photonics: optical electronics in modern communications*. 2007.
- [37] B. R. Bennett, R. A. Soref, and J. A. Del Alamo. Carrier-induced change in refractive index of InP, GaAs and InGaAsP. *IEEE Journal of Quantum Electronics*, 26(1):113–122, Jan 1990.
- [38] Weng W. Chow and Dave Depatie. Carrier-induced refractive-index change in quantum-well lasers. *Optics Letters*, 13(4):303, apr 1988.
- [39] S. Murata, A. Tomita, and A. Suzuki. Influence of free carrier plasma effect on carrier-induced refractive index change for quantum-well lasers. *IEEE Photonics Technology Letters*, 5(1):16–19, jan 1993.
- [40] O. Jamadi, F. Réveret, P. Disseix, F. Medard, J. Leymarie, A. Moreau, D. Solnyshkov, C. Deparis, M. Leroux, E. Cambril, S. Bouchoule, J. Zuniga-Perez, and G. Malpuech. Edge-emitting polariton laser and amplifier based on a ZnO waveguide. *Light: Science and Applications*, 2018.

Supporting Information

CALCULATION OF WAVEGUIDE MODES PROFILE AND GRATING COUPLED MODE ANALYSIS

The spatial profiles of the magnetic field (\mathcal{H}) for the TM mode were calculated analytically according to the method illustrated in Ref. [36]. For an asymmetric waveguide of refractive index $n_2 > n_3 > n_1$ defined in the spatial range $-t < x < 0$, with modes propagating in the z direction and infinite in y , \mathcal{H} can be written as:

$$\mathcal{H}_y(x) = \begin{cases} -C \frac{n_1^2 h}{n_2^2 q} \exp(-qx) & 0 \leq x \\ C \left(\frac{n_1^2 h}{n_2^2 q} \cos(hx) + \sin(hx) \right) & -t \leq x \leq 0 \\ C \left(\frac{n_1^2 h}{n_2^2 q} \cos(ht) + \sin(ht) \right) \exp(p(x+t)) & x \leq -t \end{cases} \quad (\text{S1})$$

Where the constants q , p and h are chosen in order to satisfy the boundary conditions of the magnetic and electric fields and the wave equation for the electric field. The constant C , instead, depends on the field's intensity. The exciton resonance in the quantum well is taken into account by using a model of Lorentz oscillator [? ?], in which the permittivity is given by:

$$\epsilon(\omega) = \epsilon_\infty \left[1 + \frac{\omega_{LT}}{\omega_{ex} - \omega - i\gamma} \right] \quad (\text{S2})$$

Where ϵ_∞ is the background dielectric constant, ω_{ex} is the resonant energy, γ is the damping rate, and ω_{LT} is the longitudinal/transverse splitting.

The insertion of a grating of refractive index n_g , height h and pitch factor Λ on top of the slab waveguide, can be treated as a perturbation of the polarization vector that couples a propagating mode with a counter-propagating one, by using the coupled-mode theory [35, 36]. In our case, the perturbation is a periodic binary modulation of the refractive index, so it can be expanded in the Fourier basis as:

$$\Delta n^2(x, z) = \Delta n^2(x) \sum_{l=-\infty}^{\infty} a_l \exp(i2\pi lz/\Lambda) \quad (\text{S3})$$

$$\Delta n^2(x) = \begin{cases} (n_g^2 - n_1^2) & 0 \leq x \leq h \\ 0 & \text{elsewhere} \end{cases} \quad a_l = \begin{cases} \frac{1}{\pi l} \sin(\pi l a) & l \neq 0 \end{cases} \quad (\text{S4})$$

If a Fourier component a_q of the grating's spatial function is comparable with a guided mode's wave-vector, i. e., if $\beta_s \approx l\pi/\Lambda$, the grating will couple the propagating mode with a counter-propagating one with opposite wave-vector, following the behavior given by the equations system:

$$\frac{dA_s^-}{dz} = i \frac{\omega\mu}{4} a_q A_s^+ e^{i2(\pi q/\Lambda - \beta_s)z} \left(\frac{\epsilon_{Au}}{\epsilon_1} - 1 \right) \int_0^h [\mathcal{H}_y^s(x)]^2 dx \quad (\text{S5})$$

$$\frac{dA_s^+}{dz} = -i \frac{\omega\mu}{4} a_q A_s^- e^{-i2(\pi q/\Lambda - \beta_s)z} \left(\frac{\epsilon_{Au}}{\epsilon_1} - 1 \right) \int_0^h [\mathcal{H}_y^s(x)]^2 dx \quad (\text{S6})$$

Which can be written in a synthetic way as:

$$\frac{dA_s^-}{dz} = \kappa A_s^+ e^{-2\Delta\beta z} \quad (\text{S7})$$

$$\frac{dA_s^+}{dz} = -\kappa A_s^- e^{2\Delta\beta z} \quad (\text{S8})$$

Where $|A^+(z)|^2$ and $|A^-(z)|^2$ are the transverse field's intensity of the propagating and counter-propagating modes, respectively, at the position z . and the constants $\Delta\beta$, and κ are given by:

$$\Delta\beta = \beta_s - \pi q/\Lambda \quad \kappa = i \frac{\omega\mu}{4} a_q \left(\frac{\epsilon_{Au}}{\epsilon_1} - 1 \right) \int_0^h [\mathcal{H}_y^s(x)]^2 dx \quad (\text{S9})$$

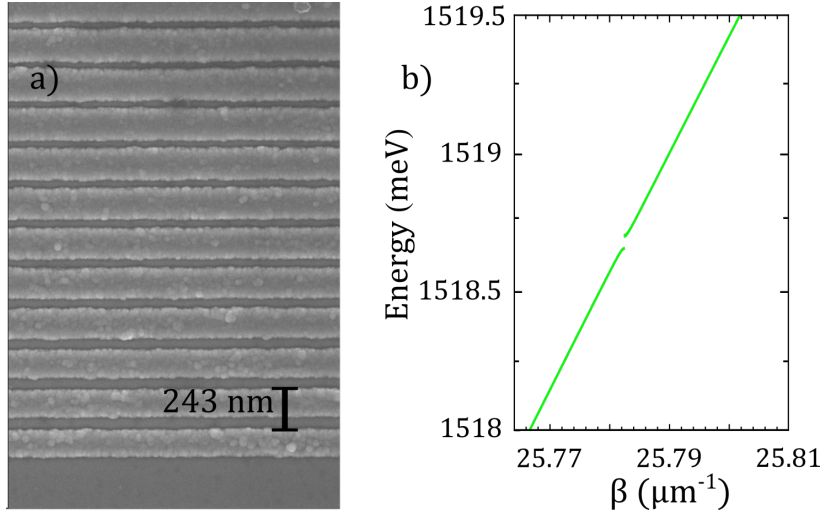


FIG. S1. **a)** SEM image of a representative gold grating in the structure. It is characterized by a pitch of 243 nm and a filling factor of 0.72. **b)** The dispersion under the grating region is perturbed, and, as a consequence, an energy gap appears in the guided mode, which implies that the grating acts as a semi-reflective mirror for those energies.

EFFECT OF THE GOLD GRATING ON THE TM POLARITONIC MODE

As a consequence of the periodic modulation of the refractive index, an energy gap centered at $\omega(\beta_s = \pi q/\Lambda)$ is generated. As illustrated in the main text, we use gold gratings 30 nm high with a filling factor comprised between 0.65 and 0.72 and a pitch of 243 nm. Fig. S1a shows a SEM image of a representative grating in the system, while the panel b of the same figure displays the dispersion relation calculated according to the method illustrated above. The existence of this gap implies that the grating acts as a semi-reflective mirror for the energies in the gap.

Figure 1 of the main text shows that the TM mode is broader than the TE mode, i.e., it is extracted with a lower angular resolution. To verify that this spread is not an intrinsic property of the waveguide, but rather a consequence of the interaction of the TM mode with the gold grating, the PL experiment is replicated, but this time, extracting the signal from a grating on top of the ITO, i.e., a less perturbative grating. As evidenced in Fig. S2, in this case both modes have comparable linewidths. This indicates that the broadening of the TM mode is a consequence of its interaction with the grating fabricated on top of the slab. It also indicates that the grating is much more perturbative for the TM mode than for the TE, in spite of the fact that the interaction is exclusively through the vanishing tail. As discussed in the main text, the stronger effect on the TM mode with respect to the TE, can be due to several effects such as a plasmonic resonance of the nanowires composing the grating or the proximity of the band gap to the excitonic resonance, the TM gap being closer to the energy range where the PL is more intense.

A direct measurement of the energy gap introduced by the gratings is done by extracting the PL through a grating 400 μm long, covering its first 100 μm with a mask in the near-field as it is described in the main text.

PROPERTIES OF THE LASER EMISSION

Figure S3 shows two main properties of the polariton laser demonstrated in this work. Figure S3a shows the full width at half maximum (FWHM) of the lasing mode as a function of the pump power (see also Figure 4 of the main text). The FWHM is reduced when the pump power is increased and it reaches a minimum just above the lasing threshold. This behaviour is well known in systems showing polariton lasing and it is explained as an increase of the coherence time above the lifetime of the polariton mode. At higher powers, a small increase of the FWHM is observed, which can be due to polariton-polariton and polariton-reservoir interactions. Figure S3b shows the overlap in the k space of the light emitted by the two gold gratings above the lasing threshold. The interference pattern is an hallmark of the first order coherence of the emitted laser light.

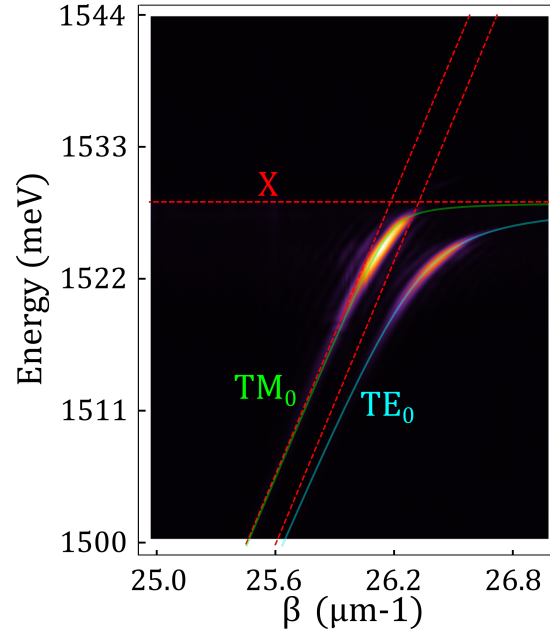


FIG. S2. PL spectrum of the guided modes extracted through a less perturbative grating, i.e. a grating on top of the ITO layer. The effect of the spread in β is suppressed.

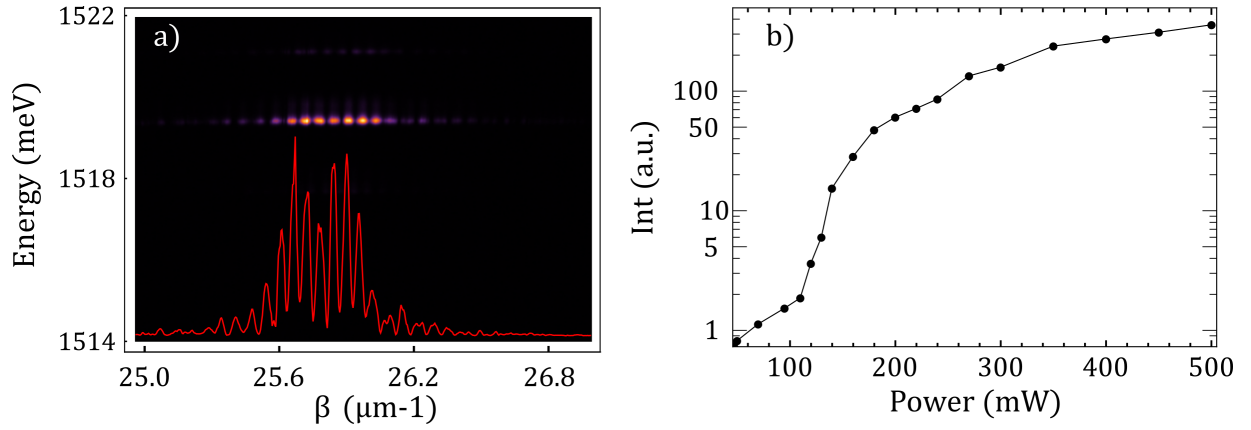


FIG. S3. **a** FWHM of the lasing mode upon increasing the pump power. A reduction in the linewidth at the lasing threshold is clearly visible. **b** Overlap in k space of the laser emission coming from the two gratings. The interference pattern results from the overlap of two coherent beams emitted by the two gratings.

TEMPORAL DYNAMICS

In this section we describe two screenshots from Supplementary Video 1 and Supplementary Video 2 and detail the way they are recorded. Each video is obtained from a k -space scan: for each k several hundreds of temporal series are acquired by using a streak camera. The set of data is then post-processed to obtain the temporal dynamics shown in the video. In other words, the data are grouped to obtain, from the intensity as a function of energy and time at a fixed k , the intensity as a function of energy and k at a fixed time. The video are then obtained as a temporal series of such Intensity vs energy and k images.

Figure S4a show a screenshot ($\tau \approx 260ps$) from Video 1. The data are acquired at an excitation power close to threshold and a series of lasing modes is still visible. The mode are in TM polarization, i.e. the polarization for which the two gold gratings act as mirrors in this configuration. Figure S4b shows the experimental configuration used to acquire the data of S4a. The pump spot (P) is placed between the two gold gratings G1 and G2 and the light is collected from the grating G2 only (black dashed line).

Figure S5a show a screenshot ($\tau \approx 200ps$) from Video 2. The data are acquired at an excitation power close to

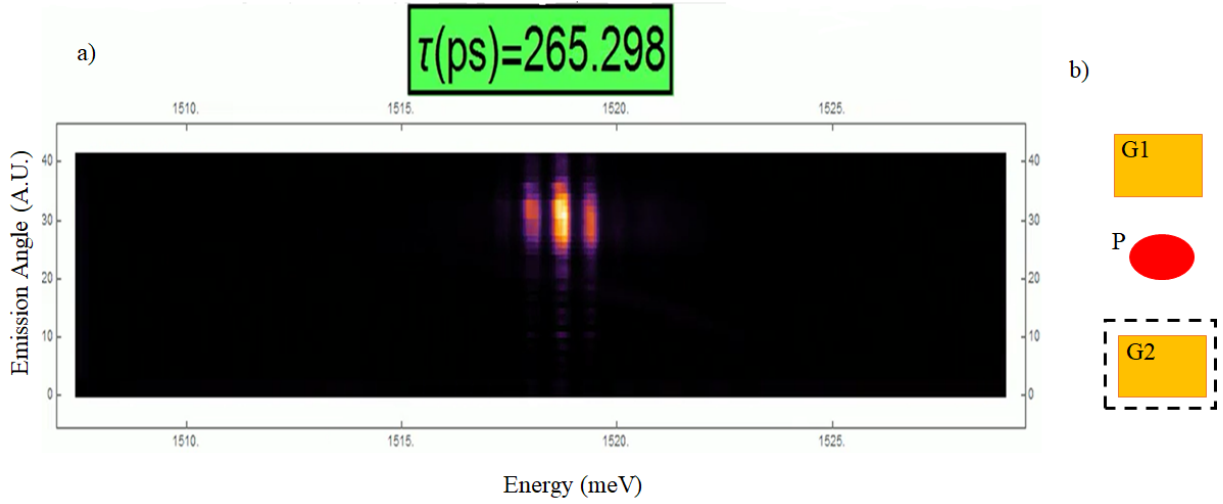


FIG. S4. **a** Screenshot from Video 1. A series of F.P modes is visible in TM polarization, i.e. the polarization for which the two gratings act as mirrors. The excitation power is here close to the lasing threshold. **b** Scheme of the configuration used to obtain the data in **a**. The pump spot (P) is placed between the two gold grating defining the F.P. cavity (G1 and G2). The light is collected only from one of the grating (black dashed line).

threshold and a series of lasing modes is still visible. In this case the light is collected from the whole cavity and the overlap in the k space produces an interference pattern. The discrete modes are in TM polarization, i.e. the polarization for which the two gold gratings act as mirrors in this configuration. Figure S5b shows the experimental configuration used to acquire the data of S5a. The pump spot (P) is placed on grating G1 and the light is collected from the whole cavity (black dashed line). Interestingly, under the pumping spot the strong coupling is initially lost then slowly recovered. On the contrary, in the region of the sample corresponding to G2, i.e. far apart from the pump spot, the mode is always in strong coupling. See for instance the TE dispersion on the bottom, coming from G2. The data shown in S4 and S5 strongly suggest that the lasing effect we report here is triggered by a spatially localized population inversion (under the pump spot) coherently populating a manifold of polariton modes.

APPLIANCE OF AN ELECTRIC FIELD

The effect of the electric field is the energy shift of the exciton peak by means of the Stark effect. As illustrated in Fig. 4a in the main text, the electric field shifts the excitonic resonance towards the modes of the Fabry-Perot resonator. As the exciton gets closer, the absorption, and hence, the quality factor of each mode is affected. At a voltage of 1.5 V the exciton peak is overlapped with the Fabry-Perot mode, increasing noticeably the absorption at this energy, and hence, reducing drastically the quality factor of the mode. Fig. S6 shows both effects. On the one hand, for applied voltages of 0.4 V and 0.9 V there is a shift of 0.02 meV and 0.12 meV, respectively. This demonstrates the possibility of a very fine tuning of the laser energy with the applied field. The spectrum corresponding to the highest applied field (1.5 V) shows how the change in the absorption peak affects the quality factor of the confined modes, inducing a spectral jump in the lasing energy, and hence, opening the possibility to use the applied electric field also as a switch to choose the desired lasing mode.

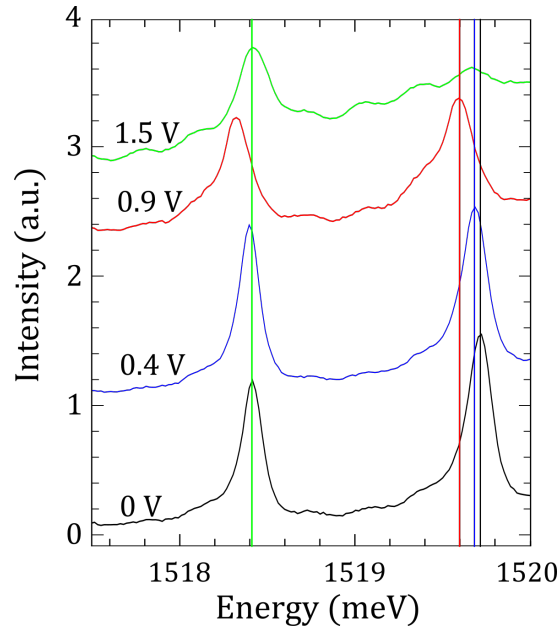
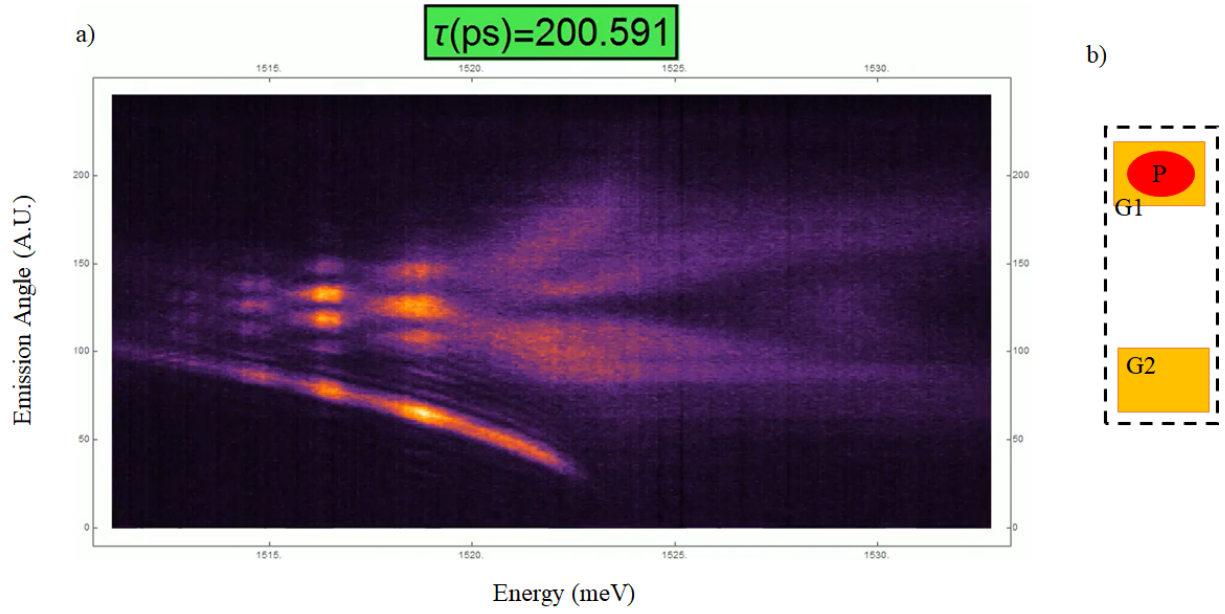


FIG. S6. By zooming the region of the cavity modes it is possible to identify the variations in the energy of the lasing mode (indicated by the vertical lines) for the different applied voltages. In the cases of 0.4 V and 0.9 V, the variation is small (0.02 meV and 0.12 meV, respectively), while in the case of 1.5 V there is an overlapping of the exciton with the bluest cavity mode; in this case the polariton lasing effect takes place in the consecutive one.